







Terahertz transient stimulated emission from doped silicon F

Cite as: APL Photonics 5, 106102 (2020); <https://doi.org/10.1063/5.0020654>

Submitted: 02 July 2020 . Accepted: 11 September 2020 . Published Online: 01 October 2020

S. G. Pavlov , N. Deßmann, A. Pohl, R. Kh. Zhukavin , T. O. Klaassen, N. V. Abrosimov , H. Riemann, B. Redlich, A. F. G. van der Meer, J.-M. Ortega, R. Prazeres , E. E. Orlova , A. V. Muraviev, V. N. Shastin, and H.-W. Hübers 

COLLECTIONS

F This paper was selected as Featured




View Online



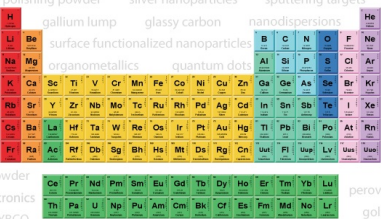
Export Citation



CrossMark



AMERICAN ELEMENTS
THE ADVANCED MATERIALS MANUFACTURER®



additive manufacturing epitaxial crystal growth cerium oxide polishing powder silver nanoparticles sputtering targets III-IV semiconductors CVD precursors europium phosphors

gallium lump glassy carbon nanodispersions InAs wafers laser crystals ultra high purity materials MOFs

surface functionalized nanoparticles organometallics quantum dot Al Si P S Cl Ar rare earth metals photovoltaics refractory metals MOCVD

superconductors transparent ceramics ultra high purity silicon

*American Elements opens up a world of possibilities so you can **Now Invent!***

Over 15,000 certified high purity laboratory chemicals, metals, & advanced materials and a state-of-the-art Research Center. Printable GHS-compliant Safety Data Sheets. Thousands of new products. And much more. All on a secure multi-language "Mobile Responsive" platform.

deposition slugs OLED Lighting spintronics solar energy AuNPs

GDC Li-ion battery electrolytes 99.999% ruthenium spheres

endohedral fullerenes copper nanoparticles diamond micropowder

CIGS MBE grade materials palladium catalysts flexible electronics

beta-barium borate borosilicate glass dysprosium pellets YBCO

pyrolytic graphite 3d graphene foam indium tin oxide mesoporous silica

raman substrates sapphire windows tungsten carbide InGaAs

barium fluoride carbon nanotubes lithium niobate scandium powder

perovskite crystals yttrium iron garnet alternative energy h-BN

gold nanocubes graphene oxide macromolecules photonics

rhodium sponge fiber optics beamsplitters infrared dyes zeolites

fused quartz metallocenes platinum ink buckyballs Ti-6Al-4V

Now Invent.™
The Next Generation of Material Science Catalogs

www.americanelements.com



Terahertz transient stimulated emission from doped silicon

Cite as: APL Photon. 5, 106102 (2020); doi: 10.1063/5.0020654
Submitted: 2 July 2020 • Accepted: 11 September 2020 •
Published Online: 1 October 2020



S. G. Pavlov,^{1,a)}  N. Deßmann,² A. Pohl,³ R. Kh. Zhukavin,⁴  T. O. Klaassen,⁵ N. V. Abrosimov,⁶ 
H. Riemann,⁶ B. Redlich,² A. F. G. van der Meer,² J.-M. Ortega,⁷ R. Prazeres,⁷  E. E. Orlova,⁸ 
A. V. Muraviev,⁹ V. N. Shastin,⁴ and H.-W. Hübers^{1,3} 

AFFILIATIONS

¹Institute of Optical Sensor Systems, German Aerospace Center (DLR), 12489 Berlin, Germany

²FELIX Laboratory, Radboud University, 6525 ED Nijmegen, The Netherlands

³Institut für Physik, Humboldt-Universität zu Berlin, 12489 Berlin, Germany

⁴Institute for Physics of Microstructures, Russian Academy of Sciences, 603950 Nizhny Novgorod, Russia

⁵Faculty of Applied Sciences, Delft University of Technology, 2628 CN Delft, The Netherlands

⁶Leibniz-Institut für Kristallzüchtung, 12489 Berlin, Germany

⁷CLIO/Université Paris-Saclay, CNRS, Institut de Chimie Physique, 91405 Orsay, France

⁸Pollard Institute, School of Electronic and Electrical Engineering, University of Leeds, LS2 9JT Leeds, United Kingdom

⁹The College of Optics and Photonics, University of Central Florida, Orlando, Florida 32816, USA

^{a)} Author to whom correspondence should be addressed: sergeij.pavlov@dlr.de

ABSTRACT

Transient-type stimulated emission in the terahertz (THz) frequency range has been achieved from phosphorus doped silicon crystals under optical excitation by a few-picosecond-long pulses generated by the infrared free electron lasers FELIX and CLIO. The analysis of the lasing threshold and emission spectra indicates that the stimulated emission occurs due to combined population inversion based lasing and stimulated Raman scattering. Giant gain has been obtained in the optically pumped silicon due to large THz cross sections of intracenter impurity transitions and resonant intracenter electronic scattering. The transient-type emission is formed under conditions when the pump pulse intervals exceed significantly the photon lifetime in the laser resonator.

© 2020 Author(s). All article content, except where otherwise noted, is licensed under a Creative Commons Attribution (CC BY) license (<http://creativecommons.org/licenses/by/4.0/>). <https://doi.org/10.1063/5.0020654>

INTRODUCTION

Transient stimulated light emission is a specific lasing mechanism when the necessary light amplification occurs during the time in which pump radiation passes an active medium. This approach is of major interest for active media where inversion (INV) population is difficult to achieve due to an inappropriate energy level structure or due to very short lifetime of the electronic states, which is, for instance, typical for extreme ultraviolet (XUV) and x-ray active media with ultrafast interstate radiative and collisional decay rates.¹ In this case, a positive feedback for the amplified light, as used in

a conventional laser, does not play a deciding significant role in generating the laser gain. The transient gain should either reach sufficiently large values of the population inversion between the involved states, such as between atomic levels in plasmas,^{1,2} or rely on transient lasing without inversion when light amplification occurs due to the specifically induced coherency between the laser states, such as those proposed for V-schemes in certain gases,^{3,4} or due to stimulated inelastic light scattering, proposed for fibers and bulk solids.^{5,6} Typical gain-length products $G \times L$, experimentally achieved in transient inversion based x-ray lasers, exceed a value of 13^7 , which is well above typical $G \times L \approx 10$ considered to be sufficient

for achieving stimulated emission. The gain length L_G , defined as the distance over which power, $\sim \exp(G \times L)$, increases by a factor of e , in the x-ray free electron lasers (FEL) reaches the $L_G \approx 1.65$ m at the soft x-ray wavelength of 15 \AA ⁸ and $L_G \approx 2.9$ m– 3.5 m at the hard x-ray wavelength of 1.5 \AA .^{8,9} The saturation length in the latter case was about 60 m ($G \times L \approx 17$).

A large pulsed gain has been measured in the active medium of terahertz (THz)-range intracenter silicon (Si) lasers under pumping with an infrared FEL.¹⁰ In a population-inversion (INV) lasing, this gain would result in $G \times L$ of up to 17 , i.e., it may support transient lasing. Such lasers can also operate using stimulated Raman scattering (SRS) of the pump light¹¹ and can also reach large Raman gain values at large pump powers. One of the important features of the transient SRS generation in the THz spectral range is a clear separation between pump (photon energies as low as 7.3 THz have been reported¹¹) and Stokes frequencies (Raman resonances in the photon energy range up to 30 THz) that can be achieved. This makes THz Si lasers different from SRS lasers in near-infrared and visible ranges (photon energies are usually larger than 300 THz), where a typical emission spectrum in the so-called “soliton Raman generation” mode can lead to merging of the pump and the Stokes shifted frequencies.¹²

Recently, it has been demonstrated that resonant pumping of a THz Si laser into particular impurity states can result in population inversion and gain at transitions between impurity states. In addition, SRS can appear as a competing process.¹³ In such a resonant pumping case, the entire physics of the process can be assigned to the dynamics of electron populations in three impurity levels of the hydrogen-like energy structure of the donor states. Due to valley-orbit splitting in a multi-valley semiconductor, the even-parity ground state is split and lifted, forming a specific structure with three $1s$ -type impurity states [$1s(A_1)$, $1s(T_2)$, and $1s(E)$] and with binding energies larger than those of the first excited odd-parity $2p_0$ and $2p_{\pm}$ impurity states (Fig. 1). The intracenter

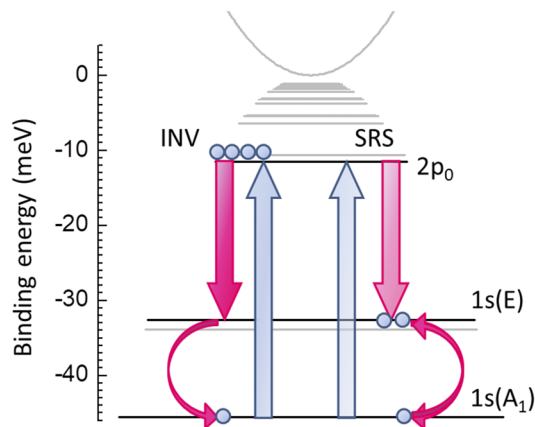


FIG. 1. Schematic diagram of lasing mechanisms utilizing the same three impurity levels in Si:P under optical pumping: (INV) inversion population-based pump photons are absorbed at the phosphorus intracenter transition $1s(A_1) \rightarrow 2p_0$ and (SRS) stimulated Raman scattering-based pump photons are scattered at Raman active phosphorus transition $1s(A_1) \leftrightarrow 1s(E)$. Circles show schematically relative population of the involved states.

$1s(A_1) \leftrightarrow 1s(E)$ transition appears to be Raman active for all group-V donors in Si.¹⁴ Three particular atomic levels in n -Si form a system where resonant pumping in an odd-parity state, namely, $1s(A_1) \rightarrow 2p_0$ or $1s(A_1) \rightarrow 2p_{\pm}$ in the case of Si:Bi,¹³ can result in simultaneous action of competing INV and SRS lasing. The main reasons why such different laser mechanisms have a gain of the same order are a resonantly enhanced Raman gain on the electronic $1s(A_1) \leftrightarrow 1s(E)$ transition and relatively low INV gain due to the short lifetime of the upper laser level in n -Si, which does not exceed $\tau \sim 200$ ps,^{15,16} along with a relatively low density of excited electrons (typical donor concentration $\sim 3 \times 10^{15} \text{ cm}^{-3}$). The co-existence of the lasing mechanisms was achieved in Si:Bi by tuning the pump photon energy in resonance with the intracenter transition. The contributions of both lasing mechanisms to the total output signal were controlled by the pump power.¹³ Under non-resonant pumping, the SRS mechanism remains with reduced gain, while INV lasing ceases.

The populations at excited impurity levels depend strongly on the storage of light at the pump and emission frequencies in the Si laser cavity as well as on the lifetimes, τ , of the electronic levels. Therefore, the feasibility of transient stimulated emission and the laser mechanism can be investigated in such a system by expanding the interpulse interval T beyond the characteristic storage time of the resonator, t_c , and the active medium, τ .

Therefore, using the time-resolving properties of an optical pump source, such as variable time intervals between the pulses or short pulse (SP) bunches, it is feasible to investigate the temporal structure of the stimulated THz emission in doped silicon and to prove the occurrence of transient lasing. To achieve this, the time intervals have to be around the characteristic range of lifetimes of the laser levels and the light in the laser cavity.

We have used a unique possibility, provided by the European FELs FELIX (Radboud University, The Netherlands) and CLIO (Institut de Chimie Physique, Orsay, France) under the EU CALIPSO Program, to investigate the temporal dynamics of THz stimulated emission from optically pumped n -Si. These FELs offer the possibility for investigating the dynamics of n -Si lasing at different temporal structures of the FEL pump pulse, namely, $6 \mu\text{s}$ – $10 \mu\text{s}$ long macropulses with interpulse intervals of $T = 1$ ns, 20 ns, and 40 ns at FELIX and $T = 16$ ns at CLIO. The other pump pulse parameters such as spectral purity, power, and micropulse (μP) temporal characteristics are almost identical for both FELs. Additionally, a short macropulse mode based on optical slicing is available at FELIX. Since the μP duration is at least one order of magnitude shorter than the lifetimes of those involved in lasing states in n -Si¹⁷ and the typical lifetime of photons in the Si laser resonator is between the μP interpulse intervals, the time-resolved investigation of n -Si lasing at different conditions will prove transient lasing of n -Si in the THz range.

Here, we report on the demonstration of transient stimulated emission from phosphorus doped silicon (Si:P) in the THz spectral range. This mode of stimulated emission occurs at the resonant intracenter pumping in the longest living odd-parity excited state of a donor, $2p_0$. Our calculations indicate relatively large gain for the resonant Raman scattering process in comparison with the population inversion mechanism for the light amplification in the transient lasing mode. This shows large gain values achieved under optical pumping of n -Si: it is worth noting that the gain is in the same order

as those realized in laser-induced high-density plasmas used in x-ray laser sources.

EXPERIMENTAL

The samples were made of Si crystals grown by the float zone technique and doped by using phosphine (SiH_3) gas. The typical concentrations of phosphorus in the samples were around $3 \times 10^{15} \text{ cm}^{-3}$. The samples were cut and optically polished in the form of rectangular parallelepipeds with typical dimensions of $5 \times 7 \times 7 \text{ mm}^3$. By this means, the crystal serves as a laser cavity on total internal reflection modes with typical lifetimes of the THz light inside the resonator in the order of $t_c \sim 10 \text{ ns}$.¹⁰ The larger facets were oriented perpendicular to the crystal growth axis, [100] or [111]. The observation of THz stimulated emission has been arranged in transverse configuration with orthogonal pump and output emission directions (Fig. 2). The *n*-Si samples were placed in a cryogenic dipstick, which was immersed in a liquid helium (LHe) transport vessel or, alternatively, in a LHe flow cryostat, and cooled to about 5 K.

A conventional setup layout used the standard μP mode, while few experiments at FELIX laboratory used a sliced mode when FEL emission passes an optical switch based on a silicon wafer irradiated by a few ns pulsed Nd:YAG laser. By such optical bandgap activation of large concentration of free charge carriers, this semiconductor plate was turned into a metal-like phase that allowed us to modulate the FEL reflection from the plate and, by this means, to cut a short pulse (SP) from the few μs long macropulse. The resulting pulse duration and shape in this sliced mode depends (on pulse front) on the SP laser shape and intensity and (on pulse tail) additionally on relaxation rate of induced electron-hole pairs in the

silicon wafer. Typical spectral linewidths of the pump emission were within 0.3%–0.5% rms of the central wavelength. The FEL linewidth exceeds the linewidth for the $1s(A_1) \rightarrow 2p_0$ impurity transition in Si:P.

Obviously, time-resolved measurements require a fast, sensitive, and broadband detector with sufficient dynamic range. This is of one the major challenges for acquisition and characterization of the transient THz lasing process. We have relied on a compromise between the detector's speed of response and its sensitivity. The detector's spectral coverage allowed performing measurements in the full spectral range (20–120 μm) with good signal-to-noise ratio and large dynamic range and at the same time to get the necessary spectral resolution in the allocated beam time. For this purpose, we used a LHe cooled Ge:Ga detector with an intrinsic response time of $\sim 1 \text{ ns}$. The bias circuitry reduced the response time to 20 ns measured with 0.5 GHz–1 GHz bandwidth digital oscilloscopes. Slower, more sensitive Ge:Ga detectors have been used for monitoring and alignment of the beams in the cryogenic dipstick. The time-resolved emission spectra of the Si:P laser were taken with a THz step-scan Fourier transform interferometer. Several averages of the detected signal were made at each acquisition step in order to minimize the pulse-to-pulse instabilities, which was the main source of noise in these measurements. Beside spatial separation, additional high optical density low-pass filters (room temperature c-cut quartz and CaF_2 as well as cold sapphire and CaF_2) have been used to dump scattered pump light.

Stimulated emission from Si:P

Stimulated emission from Si:P occurs from all samples when pumped at photon energies equal or larger than the binding energy of the $2p_0$ excited state, similar to other Si lasers.^{17,18} The Stokes shift due to electronic Raman scattering on the $1s(A_1) \leftrightarrow 1s(E)$ transition in the Si:P laser is $\sim 3.15 \text{ THz}$ (13.028 meV)¹⁸ and the lowest pump photon energy into the long-lived odd-parity state, $1s(A_1) \rightarrow 2p_0$, is $\sim 8.24 \text{ THz}$ (34.109 meV)¹⁸. Figure 3 shows the dependence of the integrated lasing intensity on the pump photon energy (the so-called lasing spectrum) at different micropulse intervals T . Pumping at impurity resonances [$1s(A_1) \rightarrow p$ states] corresponds to the cases of both INV lasing and SRS lasing. SRS lasing occurs also when pumped between the impurity states. The lowest lasing threshold occurs under resonant pumping in the long-lived $2p_0$ state for INV as well as SRS lasing, and the largest lasing threshold is for SRS lasing emission when pumped between the $2p_0$ and $2s(T_2)$ states (Fig. 3). The slopes at the lasing thresholds at impurity resonance remain unchanged for $T \geq 20 \text{ ns}$ when the off-resonance SRS lasing bands vanish.

At 1 GHz ($T = 1 \text{ ns}$) μP repetition rate, the temporal behavior of Si:P emission was not resolved by the Ge:Ga detectors. The Si:P emission spectra are the same as earlier reported:^{17,18} resonant pumping in odd-parity np states ($n = 2, 3, \dots$) results in emission on the $2p_0 \rightarrow 1s(E)$ transition (when pumped into the $2p_0$ state) or on the $2p_0 \rightarrow 1s(T_2)$ transition. Pumping in the spectral range corresponding to the intracenter transition between the $2p_0$ and the $3p_0$ states results in SRS lasing. Some particular features in the emission spectra are caused by atmospheric absorption [Fig. 3(b)] and interfere especially with the SRS lasing at high laser thresholds.

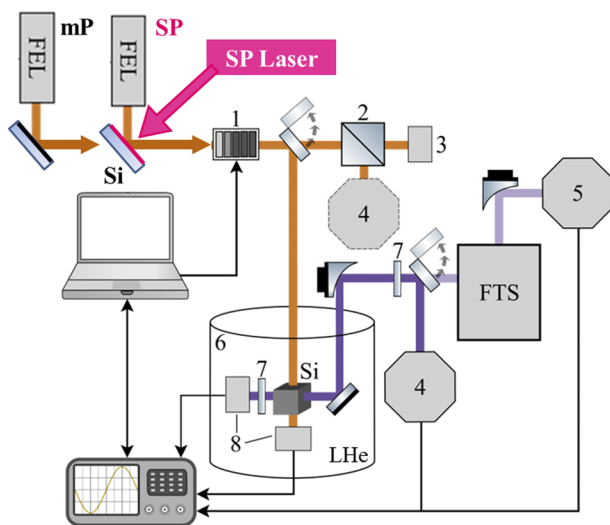


FIG. 2. Schematic diagram of the optical pumping setup: (mP) conventional macropulse operation mode and (SP) short pulse sliced mode (FELIX). 1—FEL attenuator, 2—beam splitter, 3—FEL power meter, 4 and 5—Ge:Ga fast detector, 6—cryogenic vessel/cryostat, 7—low-pass filters, and 8—Ge:Ga detectors.

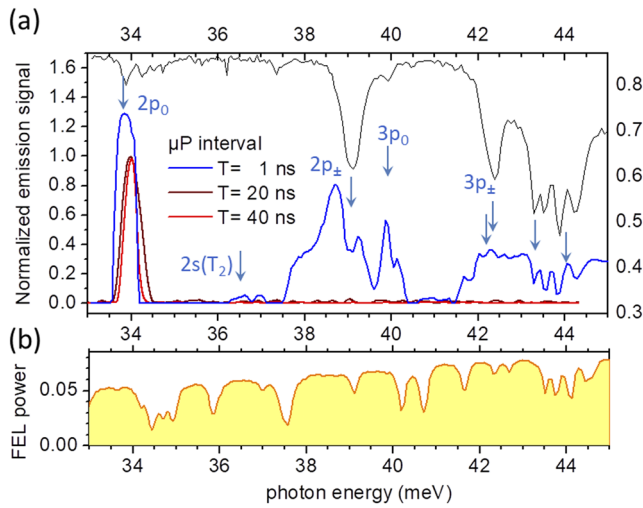


FIG. 3. (a) Si:P lasing pump spectrum at three different μP intervals and at about the same μP energy. The upper plot shows the FEL signal intensity passing through the Si:P sample. The arrows indicate impurity resonances. The symbols at the arrows are given for the impurity transitions with the largest oscillator strengths. The macropulse duration is about $6 \mu\text{s}$ (FWHM). The off-resonant broad-band lasing emission bands, which are characteristic for SRS, remain only at $T = 1 \text{ ns}$. (b) FEL power spectrum. The fine structure is caused by atmospheric absorption in the laboratory.

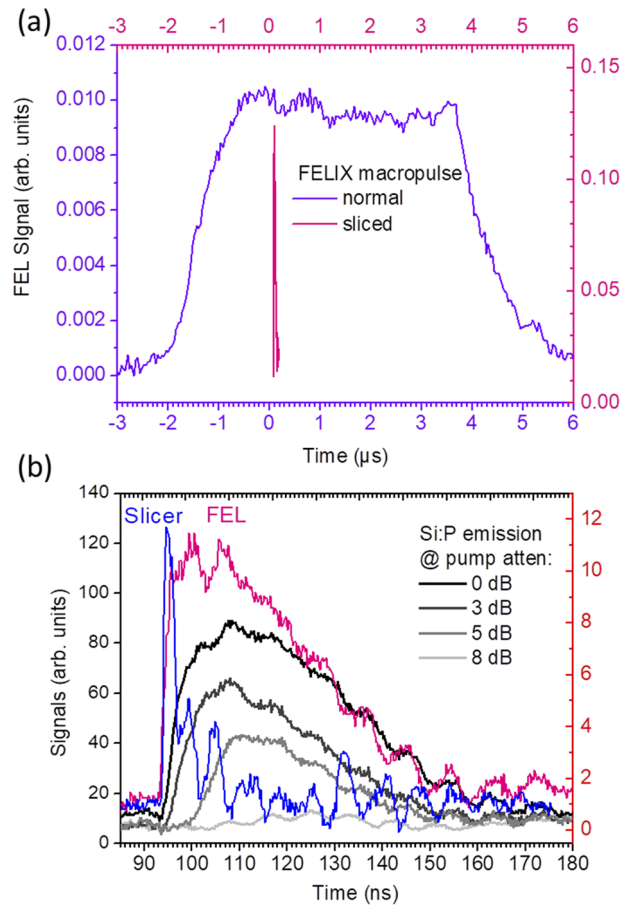


FIG. 4. (a) FELIX pump pulses in the regular ($\sim 4 \mu\text{s}$) macropulse and sliced ($\sim 20 \text{ ns}$) modes. The micropulse separation is $T = 1 \text{ ns}$. (b) FELIX pump pulse in the sliced mode and Si:P laser emission pulses in the sliced mode, $T = 1 \text{ ns}$, for different pump powers (attenuation corresponds to the pulses from the top downwards). The ripples on the pulses are due to mismatch in the detector's electric circuit (10 GHz sampling rate of the oscilloscope).

Since the FELIX macropulse in the regular operation regime ($6 \mu\text{s}$ – $10 \mu\text{s}$, 5 Hz or 10 Hz repetition rate) has a typical quasi-trapezoidal shape with a relative long build-up time (Fig. 4), it complicates an accurate determination of the THz gain in *n*-Si, when estimated on the basis of the signal growth at the beginning of the emission macropulse. To minimize such an inaccuracy, we have used the FELIX facility option of sliced operation with the time gating determined by an optical switch. Such a mode provides a short pulse with sharp pulse front. The slicer timing was chosen to cut off the relatively flat saturated macropulse part [Fig. 4(a)]. This provided in our experiments the macropulse with a duration only slightly larger than photon lifetime in the resonator and at reduced by the factor ~ 20 to regular mode μP peak power. The SP lasing mode had about 15 micropulses (of total ~ 20) with about the same peak intensity. The $L_G = 50 \pm 5 \text{ cm}$ was estimated from the exponential growth of the emission macropulse at lowest pump powers (in terms of Si:P emission detectivity, at 10 dB FEL attenuation) [Fig. 4(b)] in optically pumped Si:P at $36.35 \mu\text{m}$ (resonantly in the $2p_0$ phosphorus state with a $\sim 120 \text{ nJ}$ sliced macropulse). Note that at such gain length, transient stimulated emission in the Si:P samples cannot occur. An accurate estimate of the gain at larger (a factor 10 available) pump powers failed due to the strong nonlinear increase in the output power.

At 25 MHz and 50 MHz μP repetition rate ($T = 40 \text{ ns}$ and 20 ns), lasing has been observed only when pumped within a narrow spectral band centered at a donor transition in the long-lived $2p_0$ state. The temporal behavior of the Si:P emission is resolved from $T \geq 16 \text{ ns}$. At $T = 40 \text{ ns}$, Si:P emission with clear μP separation has been observed (Fig. 5). THz lasing starts with a delay to the pump pulse up

to about $1 \mu\text{s}$ at $T = 40 \text{ ns}$. This is a typical feature of the SRS lasing with gain following the FEL μP power reaching its maximum at the FEL gain saturation level (at the macropulse quasi-flat top). Stimulated emission from Si:P shows a longer decay compared to the FEL pump pulse. The gain length in optically pumped Si:P at $36.35 \mu\text{m}$ (resonantly in the $2p_0$ phosphorus state with a $\sim 250 \text{ nJ}$ macropulse, $\sim 180 \mu\text{P}$ in 25 MHz mode) was estimated from the exponential growth of the emission macropulse at 10 dB pump power as $L_G = 6 \pm 1 \text{ cm}$. Obviously, for the case of Raman-type stimulated emission, the gain can exceed the values necessary to obtain a gain-length product above 5–7 because it is proportional to the pump power.

The slope efficiency for lasing on the $2p_0 \rightarrow 1s(E)$ transition is the same for μP separations of 20 ns and 40 ns, while it is smaller for $T = 1 \text{ ns}$ (Fig. 6). This supports the assumption that the Si lasing may have a qualitative change when the intervals between pump

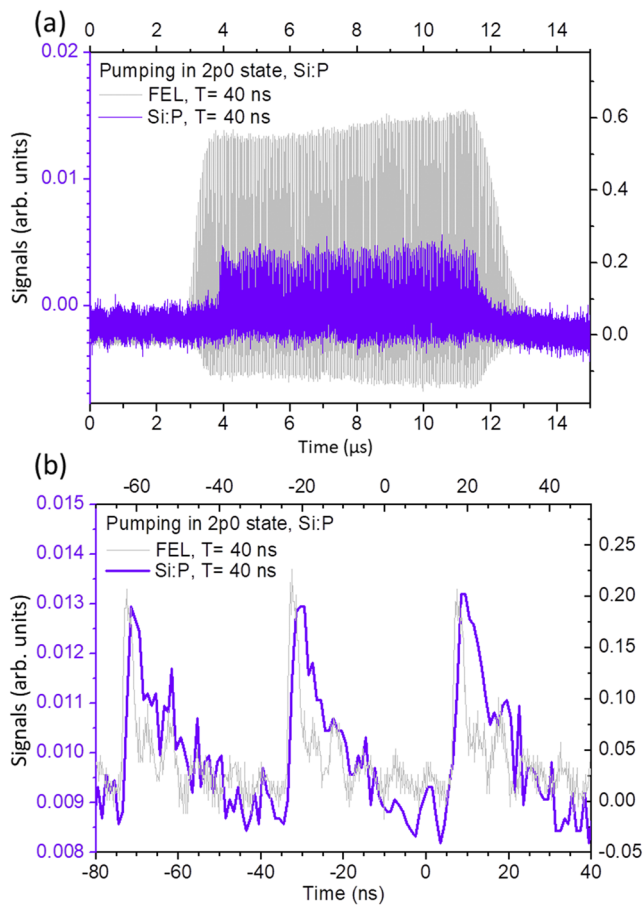


FIG. 5. FEL pump and Si:P laser emission pulses for resonant pumping in the $2p_0$ phosphorus state at $T = 40$ ns: (a) Full macropulse, full 10 GHz sampling rate (oscilloscope)—note a ~ 1 μ s delay of the Si:P emission pulse relative to the FEL pump pulse, and (b) several micropulses of the FEL and the Si:P laser. The sampling rate in the Si:P emission channel is 1 GHz. FEL and Si:P laser emission pulses have a relative shift due to different optical path lengths to the measurement points. The ripples on the pulses are due to mismatch in the detector circuits.

pulses are smaller or larger than the photon lifetime in the laser cavity, which is around 10 ns. The absolute value of the laser threshold increases by almost an order of magnitude from $T = 1$ ns–20 ns but does not change from $T = 20$ ns–40 ns.

The emission spectra of the Si:P laser pumped on the $1s(A_1) \rightarrow 2p_0$ transition do not change significantly by changing the μ P interval (Fig. 7). The typical emission spectrum is relatively broad at maximum pump power (~ 250 nJ per ~ 180 μ P) at $T = 40$ ns and 20 ns and ~ 12 μ J per ~ 7000 μ P) at $T = 1$ ns) matching with the linewidth of a pump source. Such a broad emission spectrum is a feature of SRS lasing.¹⁷ The spectral dip at 21.13 meV fits well to an absorption line of water vapor, unavoidable in our experiments, and indicates on Raman lasing, which mirrors the pump spectrum. At a reduced pump power, the emission spectrum for $T = 1$ ns narrows a bit with a peak centered on the $2p_0 \rightarrow 1s(E)$ transition, similar to previously reported data.¹⁷ A slight detuning of the FEL pump frequency from

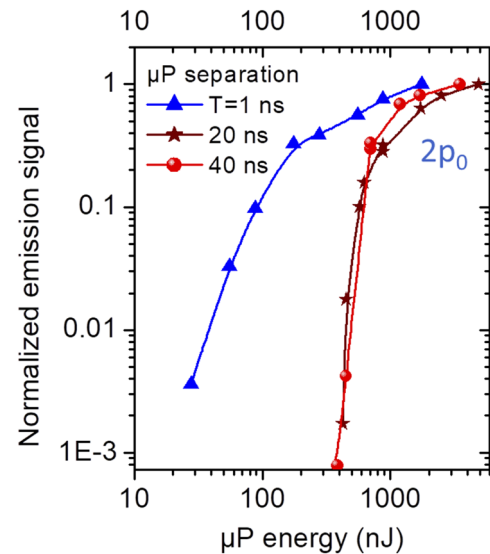


FIG. 6. Si:P laser thresholds at different μ P intervals for resonant pumping in the $2p_0$ phosphorus state.

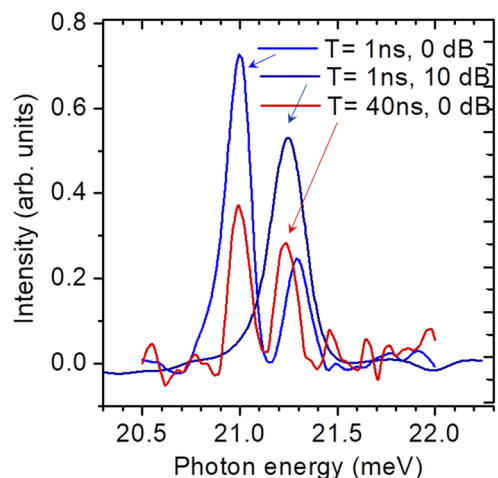


FIG. 7. Si:P laser emission spectra at different μ P intervals and pump power attenuation. Resonant pumping is in the $2p_0$ phosphorus state.

out of resonance for $T = 1$ ns results in a shift of the spectrum, which is equal to the pump photon energy shift, as it is expected in the case of SRS lasing.

The Si:P laser dynamics at the macropulse rise and its emission spectra indicate on SRS lasing as the dominating mechanism at most of the FEL pump parameters.

Simulation of the laser mode dynamics

In order to obtain a thorough understanding of the lasing dynamics, in particular on the contributions of INV and SRS, we

have carried out simulations of the dynamical processes in the active medium using parameters, which are typical for our experiments. We have applied a simplified model of nonstationary balance equations for the three-level system [$1 \equiv 1s(A_1)$, $2 \equiv 1s(E)$, $3 \equiv 2p_0$] with populations n_1 , n_2 , and n_3 , and photon fluxes at two close frequencies [$N'(\omega'_{32})$, $N(\omega_{32})$]—photon fluxes for Raman and INV lasing photons at energies $\hbar\omega'_{32} \approx \hbar\omega_{32}$. We further assume resonant pumping into level 3. This yields the following set of equations:

$$\begin{aligned} \frac{dn_1}{dt} &= -W_L \times n_1 + W_{21} \times n_2 - (n_1 - n_2) \times \sigma_R \times N_{32}(\omega'_{32}), \\ \frac{dn_2}{dt} &= -W_{21} \times n_2 + W_{32} \times n_3 + (n_3 - n_2) \times \sigma_{32} \times N_{32}(\omega_{32}) \\ &\quad + (n_1 - n_2) \times \sigma_R \times N'_{32}(\omega'_{32}), \\ \frac{dn_3}{dt} &= -W_{32} \times n_3 + W_L \times n_1 - (n_3 - n_2) \times \sigma_{32} \times N_{32}(\omega_{32}), \\ \frac{dN(\omega_{32})}{dt} &= (n_3 - n_2) \times \sigma_{32} \times N_{32}(\omega_{32}) - N_{32}(\omega_{32})/t_c, \\ \frac{dN'(\omega'_{32})}{dt} &= (n_1 - n_2) \times \sigma_R \times N'_{32}(\omega'_{32}) - N'_{32}(\omega'_{32})/t'_c, \\ n_1 + n_2 + n_3 &= N, \end{aligned} \quad (1)$$

where $W_L = N_{\text{pump}} \times \sigma_{13}$ is the pump rate into the upper laser level 3, where N_{pump} is the pump photon flux and σ_{13} is the absorption cross section of the transition $1 \rightarrow 3$, W_{21} and W_{32} are nonradiative decay rates between corresponding levels, σ_{32} is the cross section for the dipole allowed optical transition between level 3 and 2, $\sigma_R \sim W_L \times \sigma_{32}$ is the stimulated electronic Raman cross section, which is derived from the Raman gain equation given in Ref. 19 for a resonant Raman transition between levels 1 and 2 with the SRS output photon energy $\hbar\omega_{32}$, and t'_c and t_c are the effective photon lifetimes in the resonator cavity for Raman and INV lasing photons and considered to be equal. We chose the following parameters according to the empirical data: decay rates $W_{32} = 1/\tau_{32} \sim (200 \text{ ps})^{-1}$ ¹⁶ and $W_{21} = 1/\tau_{21} \sim (10 \text{ ps})^{-1}$,²⁰ cross sections $\sigma_{13} = \sigma_{32} = 4 \times 10^{-15} \text{ cm}^2$,²¹ σ_R was chosen to be equal to the σ_{13} at the pump rate $W_L = 1.6 \times 10^{25} \text{ cm}^{-2} \text{ s}^{-1}$, $t_c \sim 10 \text{ ns}$,¹⁰ and the donor concentration is $N = 3 \times 10^{15} \text{ cm}^{-3}$. The pump rate (FEL photon flux) has been chosen as a parameter in the calculations. By varying the pump rate, three different major cases can be distinguished: (i) INV lasing only at very low pump rates, just above the INV laser threshold, (ii) simultaneous INV and SRS lasing at pump rates exceeding the SRS lasing threshold, and (iii) dominating SRS compared to INV lasing at large pump rates.

The modeling results for pumping with the sliced FEL pulse [Fig. 8(b)] show that both lasing mechanisms can occur at a pump rate in the range of the experimental values. The INV gain envelope mirrors the pump macropulse shape in the entire time range. The SRS gain follows this shape after the macropulse peak maximum is chosen to be at 13 ns. Steady-type regime is not building in this case, which is expected in the situation with macropulse duration of a few t_c .

Since most of data, including the emission spectra, were collected at pump powers far above the lasing thresholds in various μP separation modes and considering the experimentally observed macropulse shape and spectral features, we assume that both lasing mechanisms, SRS and INV, occur simultaneously. Typical modeling data for the conditions corresponding to simultaneous lasing mechanisms, i.e., corresponding to the case that threshold for SRS is exceeded, are summarized in Figs. 8 and 9. All major changes occur

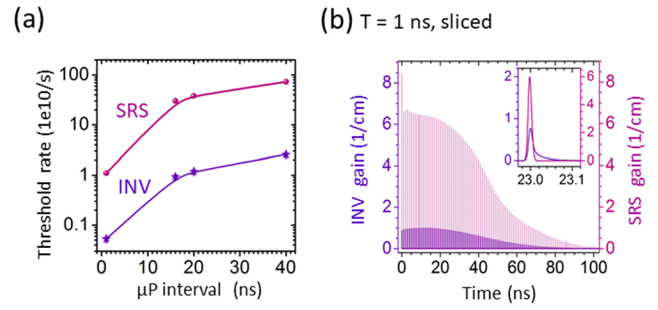


FIG. 8. The sliced 1 GHz FEL operation mode, calculated: (a) lasing thresholds for INV (violet) and SRS (magenta) contributions and (b) INV (violet) and SRS (magenta) gain. Pump rate $W_L = 8 \times 10^{10} \text{ s}^{-1}$.

only at the front part of the macropulse, and therefore, we plot the macropulse in the time range covering this dynamics.

There are a few important features we will focus on. First, the laser gain for both mechanisms does not stay until the next pump micropulse: The SRS gain that is proportional to the product of the

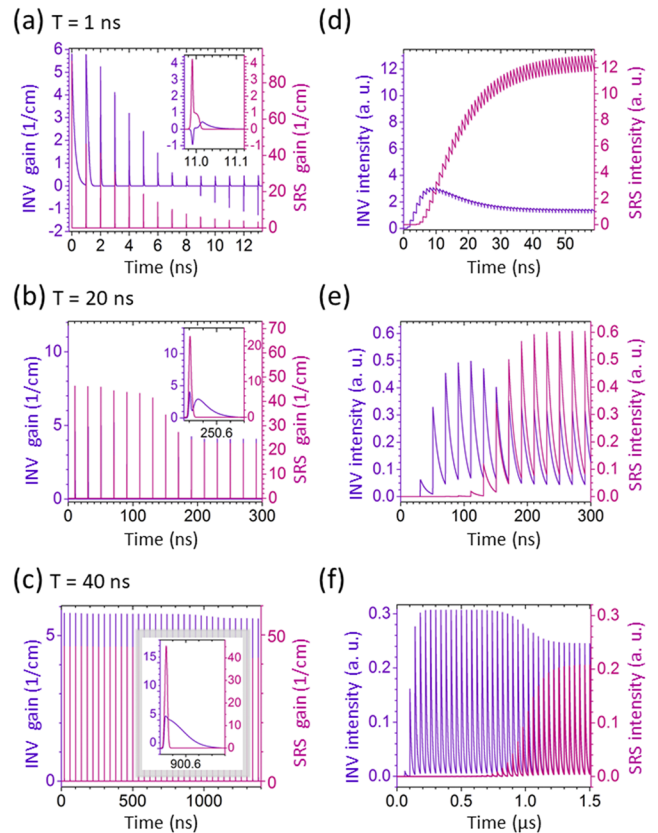


FIG. 9. [(a)–(c)] Calculated gain of INV (violet) and SRS (magenta) lasing for pump pulse intervals of 1 ns, 20 ns, and 40 ns. The insets show the gain for a single μP . [(d)–(f)] Calculated emission signals on time scales where quasi-steady lasing is reached at μP intervals of 1 ns, 20 ns, and 40 ns. Pump rate $W_L = 8 \times 10^{10} \text{ s}^{-1}$.

FEL μ P-shape and population inversion, $FEL(t) \times (n_2(t) - n_1(t))$, vanishes on the scale of the FEL μ P duration. The INV gain that is proportional to $(n_3(t) - n_2(t))$ is slightly longer than the μ P, but not more than 200 ps.

At $T = 1$ ns, INV and SRS lasing show the strongest competition, which is clearly visible on the 100 ps-scale [see the inset in Fig. 9(a)] and also on the macropulse time scale [see Figs. 9(d)–9(f)]. The μ P-scale dynamics remains pronounced in the 1 ns periodic fringes of the macropulse output [Fig. 9(d)]. The time scale for building up the emission is a few ten ns, and after that, a quasi-steady mode is reached. This is not the case for the sliced operation with $T = 1$ ns, where laser gain and output vary until the end of the macropulse. In a quasi-steady-state, gain values are significantly reduced and the output powers are maximized. Obviously, the laser photons, which are trapped in the cavity between two consecutive pump pulses ($T < t_c$), provide the positive feedback for the stimulated emission and strongly affect the laser level populations, therefore contributing to the quasi-continuous laser emission.

At $T > 1$ ns, the influence of the trapped photons becomes smaller for larger T for INV as well as for SRS lasing. The laser intensity decreases slowly, the μ P gain and the ps-scale dynamics vanish, and SRS lasing requires a significantly longer time, up to 1 μ s, to reach the quasi-steady regime. The output emission exhibits quasi-transient dynamics and the lasing photon density vanishes until the next pump pulse. The peak gain-length products in this mode are about 35–70 (SRS) and 7–10 (INV) for μ P intervals of 20 ns and 40 ns, respectively. These large values are close to the experimentally observed values for the transient gain, which are necessary for the stimulated transient emission for the INV case,^{7–9} and are in the order of saturation values for the SRS case.

Note here that certain margins for inputs into the model should be considered because of uncertainties in some parameters, such as the lifetimes of the involved impurity states and the integrated Raman cross section. The latter might be underestimated due to the spectral width of the pump pulse. Since the FEL spectrum has a spectral width larger than the linewidth of the pumped impurity transition, only spectrally overlapping photons contribute to the INV gain, while in the case of stimulated Raman emission, all FEL photons in vicinity of an impurity resonance take part in the stimulated Raman scattering and can contribute to the total SRS gain, which is spectrally broader than the gain of INV lasing process.

This modeling shows a pronounced qualitative change in the laser thresholds and dynamics when the interpulse intervals exceed the photon lifetime in the cavity, because of the loss of positive feedback. Population inversion lasing occurs at all micro-pulse intervals. On the other hand, the reduction in the photon lifetime in the cavity changes the partial contribution of SRS lasing. Also, detuning from the impurity resonance causes a stronger reduction of the pump cross section for the INV laser as compared to the SRS case.

CONCLUSIONS

The spectral and dynamical characteristics of the observed THz stimulated emission from Si:P pumped by infrared ps-pulses from a FEL reveal a transient lasing mode when the pump pulse intervals exceed the photon lifetime in the Si:P laser cavity. Both experiments and simulations show a pronounced micropulse structure of the

laser gain as well as the laser output power at pump pulse intervals of 40 ns.

The relatively long (~ 10 ns) laser cavity photon lifetime enables strong competition between two laser mechanisms based on population inversion or stimulated Raman scattering and results in a time-shape of the laser output that follows the pump macropulse at 1 ns pump interval.

At larger pump pulse intervals, the emission pulses from the Si:P laser are resolved. The experimental data on the lasing thresholds indicate that such a mode occurs already at intervals exceeding 16 ns, while the calculations indicate a gradual evolution of the temporal behavior with increasing micropulse intervals. Even at the largest interval of 40 ns, stimulated emission based on population inversion dominates Raman type emission in the vicinity of the laser threshold. For pump intensities well above the thresholds, the simulated gain for stimulated Raman emission exceeds the one for the population inversion and both lasing mechanisms co-exist during almost the entire macropulse. In most of our experiments, at the largest pump pulse intervals, stimulated Raman emission dominates. This indicates a giant Raman gain as calculated at pump rates significantly above the SRS lasing threshold.

The demonstrated transient lasing mode implies a large pulsed gain built-up during the few-ps long pump pulse. For the case of stimulated Raman emission, the simulation yields gain values up to 40 cm^{-1} , while for the case of population inversion-based lasing, it is above 5 cm^{-1} . The latter is very similar to the experimentally measured pulsed gain for the INV Si:P laser.¹⁰ Such gain values profit from the large optical cross sections of intracenter impurity transitions ($\sim 10^{-14} \text{ cm}^2$) and resonant intracenter Raman scattering.

To summarize, the large infrared dipole and Raman cross sections at impurity resonances in semiconductors can be effectively used under optical pumping for ultrafast buildup a large gain in the THz frequency range sufficient for transient picosecond stimulated emission.

ACKNOWLEDGMENTS

The authors are greatly indebted to J. N. Hovenier, who contributed to the initial experiments and sadly passed away. We lost a great colleague. This research was supported through the EC CALIPSO program for the transnational access to the European FELs and synchrotron facilities. This work was partly supported by joint research project of Russian Foundation for Basic Research and Deutsche Forschungsgemeinschaft (Grant Nos. DFG 389056032 and RFBR 18-502-12077-DFG).

DATA AVAILABILITY

The data that support the findings of this study are available from the corresponding author upon reasonable request.

REFERENCES

- 1P. K. Jha, A. A. Svidzinsky, and M. O. Scully, "Coherence enhanced transient lasing in XUV regime," *Laser Phys. Lett.* **9**, 368 (2012).
- 2R. A. Ganeev, A. Ishizawa, T. Kanai, T. Ozaki, and H. Kuroda, "Coherent soft x-ray lasing from Ni-like Mo plasma in transient gain amplification scheme," in *2003*

European Quantum Electronics Conference (IEEE Cat No. 03TH8665), Munich, Germany, 22–27 June 2003 (IEEE, 2003), Vol. 441.

³A. A. Svidzinsky, L. Yuan, and M. O. Scully, “Transient lasing without inversion,” *New J. Phys.* **15**, 053044 (2013).

⁴L. Yuan, D.-W. Wang, Ch. O’Brien, A. A. Svidzinsky, and M. O. Scully, “Sideband generation of transient lasing without population inversion,” *Phys. Rev. A* **90**, 023836 (2014).

⁵P. G. May and W. Sibbett, “Transient stimulated Raman scattering of femtosecond laser pulses,” *Appl. Phys. Lett.* **43**, 624 (1983).

⁶S. N. Smetanin, “Transient stimulated Raman scattering in crystals during motion of populations of vibrational states,” *J. Exp. Theor. Phys.* **119**, 36 (2014).

⁷M. Kozlova, J. Nejdil, M. Albrecht, S. Sebban, J. Gautier, K. Ta Phuoc, A. Klisnick, A. Le Marec, and F. Tissandier, “Overview of development of laser driven secondary sources at PALS and ELI,” in *X-Ray Lasers*, Springer Proceedings in Physics Vol 169, edited by J. Rocca, C. Menoni, and M. Marconi (Springer, Cham, 2014), pp. 35–43.

⁸D. Ratner, D. A. Brachmann, F. J. Decker, Y. Ding, D. Dowell, P. Emma, J. Frisch, S. Gilevich, G. Hays, P. Hering, Z. Huang, R. Iverson, H. Loos, A. Miahnahri, H. D. Nuhn, J. Turner, J. Welch, W. White, J. Wu, D. Xiang, G. Yocky, and W. M. Fawley, “FEL gain length and taper measurements at LCLS,” in *Proceedings of the 2009 Free-Electron Laser Conference*, Liverpool, UK, 23–28 August 2009, <http://www.jacow.org>, pp. 221–224.

⁹P. Emma, R. Akre, J. Arthur, R. Bionta, C. Bostedt, J. Bozek, A. Brachmann, P. Bucksbaum, R. Coffee, F.-J. Decker, Y. Ding, D. Dowell, S. Edstrom, A. Fisher, J. Frisch, S. Gilevich, J. Hastings, G. Hays, Ph. Hering, Z. Huang, R. Iverson, H. Loos, M. Messerschmidt, A. Miahnahri, S. Moeller, H.-D. Nuhn, G. Pile, D. Ratner, J. Rzepiela, D. Schultz, T. Smith, P. Stefan, H. Tompkins, J. Turner, J. Welch, W. White, J. Wu, G. Yocky, and J. Galayda, “First lasing and operation of an Ångstrom-wavelength free-electron laser,” *Nat. Photon* **4**, 641–647 (2010).

¹⁰R. Kh. Zhukavin, V. N. Shastin, S. G. Pavlov, H.-W. Hübers, J. N. Hovenier, T. O. Klaassen, and A. F. G. van der Meer, “Terahertz gain on shallow donor transitions in silicon,” *J. Appl. Phys.* **102**, 093104 (2007).

¹¹S. G. Pavlov, H.-W. Hübers, J. N. Hovenier, T. O. Klaassen, D. A. Carder, P. J. Phillips, B. Redlich, H. Riemann, R. Kh. Zhukavin, and V. N. Shastin, “Stimulated

terahertz Stokes emission of silicon crystals doped with antimony donors,” *Phys. Rev. Lett.* **96**, 037404 (2006).

¹²K. J. Blow and D. Wood, “Theoretical description of transient stimulated Raman scattering in optical fibers,” *IEEE J. Quantum Electron.* **25**, 2665 (1989).

¹³S. G. Pavlov, N. Defßmann, B. Redlich, A. F. G. van der Meer, N. V. Abrosimov, H. Riemann, R. Kh. Zhukavin, V. N. Shastin, and H.-W. Hübers, “Competing inversion-based lasing and Raman lasing in doped silicon,” *Phys. Rev. X* **8**, 041003 (2018).

¹⁴K. Jain, S. Lai, and M. V. Klein, “Electronic Raman scattering and the metal-insulator transition in doped silicon,” *Phys. Rev. B* **13**, 5448–5464 (1976).

¹⁵N. Q. Vinh, P. T. Greenland, K. Litvinenko, B. Redlich, A. F. G. van der Meer, S. A. Lynch, M. Warner, A. M. Stoneham, G. Aeppli, D. J. Paul, C. R. Pidgeon, and B. N. Murdin, “Silicon as a model ion trap: Time domain measurements of donor Rydberg states,” *Proc. Natl. Acad. Sci. U. S. A.* **105**, 10649 (2008).

¹⁶H.-W. Hübers, S. G. Pavlov, S. A. Lynch, P. T. Greenland, K. L. Litvinenko, B. Murdin, B. Redlich, A. F. G. van der Meer, H. Riemann, N. V. Abrosimov, P. Becker, H.-J. Pohl, R. Kh. Zhukavin, and V. N. Shastin, “Isotope effect on the lifetime of the $2p_0$ state in phosphorus-doped silicon,” *Phys. Rev. B* **88**, 035201 (2013).

¹⁷S. G. Pavlov, R. Kh. Zhukavin, V. N. Shastin, and H.-W. Hübers, “The physical principles of terahertz silicon lasers based on intracenter transitions,” *Phys. Status Solidi B* **250**, 9 (2013).

¹⁸S. G. Pavlov, H.-W. Hübers, U. Böttger, R. Kh. Zhukavin, V. N. Shastin, J. N. Hovenier, B. Redlich, N. V. Abrosimov, and H. Riemann, “Terahertz Raman laser based on silicon doped with phosphorus,” *Appl. Phys. Lett.* **92**, 091111 (2008).

¹⁹J. B. Khurgin, “Comparative analysis of optically pumped intersubband lasers and intersubband Raman oscillators,” *J. Appl. Phys.* **78**, 7398 (1995).

²⁰V. V. Tsyplenkov, E. V. Demidov, K. A. Kovalevsky, and V. N. Shastin, “Relaxation of excited donor states in silicon with emission of intervalley phonons,” *Semiconductors* **42**, 1016 (2008).

²¹M. Porrini, M. G. Pretto, R. Scala, A. V. Batunina, H. C. Alt, and R. Wolf, “Measurement of boron and phosphorus concentration in silicon by low-temperature FTIR spectroscopy,” *Appl. Phys. A* **81**, 1187 (2005).